Article

Yearly Elevation Change and Surface Velocity Revealed from Two UAV Surveys at Baishui River Glacier No. 1, Yulong Snow Mountain

Leiyu Li [1,2], **Yuande Yang** [1,2,*], **Shijin Wang** [3], **Chuya Wang** [1,2], **Qihua Wang** [1,2], **Yuqiao Chen** [1,2], **Junhao Wang** [1,2], **Songtao Ai** [1,2] and **Yanjun Che** [4]

[1] Chinese Antarctic Center of Surveying and Mapping, Wuhan University, Wuhan 430079, China; 2016301610132@whu.edu.cn (L.L.); chuya0905@whu.edu.cn (C.W.); qhwang@whu.edu.cn (Q.W.); chenyq_my@whu.edu.cn (Y.C.); jh_wang@whu.edu.cn (J.W.); ast@whu.edu.cn (S.A.)

[2] Key Laboratory of Polar Environment Monitoring and Public Governance, Ministry of Education, Wuhan 430079, China

[3] Yulong Snow Mountain Cryosphere and Sustainable Development Observation and Research Station/State Key Laboratory of Cryospheric Sciences, Northwest Institute of Eco-Environment and Resources, Chinese Academy of Sciences, Lanzhou 730000, China; wangshijin@lzb.ac.cn

[4] Department of Geography Science, Yichun University, Yichun 336000, China; cheyanjun@jxycu.edu.cn

* Correspondence: yuandeyang@whu.edu.cn

Abstract: Glaciers play an important role in understanding the climate, water resources, and surrounding natural change. Baishui River Glacier No. 1, a temperate glacier in the monsoon-influenced Southeastern Qinghai–Tibet Plateau, has experienced significant ablation due to regional warming during the past few decades. However, little is known about the yearly changes in Baishui River Glacier No. 1. To investigate how Baishui River Glacier No. 1 has changed in recent years, digital orthophoto maps and digital elevation models were obtained from an unmanned aerial vehicle on 20 October 2018 and 22 July 2021, covering 84% and 47% of the total area, respectively. The results of the Baishui River Glacier No. 1 changes were obtained by differencing the digital elevation models, manual tracking, and terminus-retreat calculation methods. Our results showed that the surveyed area had a mean elevation change of −4.26 m during 2018 and 2021, and the lower area lost more ice than other areas. The terminus of Baishui River Glacier No. 1 has retreated by 16.35 m/a on average, exhibiting spatial variation with latitude. Moreover, we initially found that there was a high correlation between surface velocity and elevation gradient in this high-speed glacier. The surface velocity of Baishui River Glacier No. 1 was derived with the manual feature tracking method and ranged from 10.48 to 32.00 m/a, which is slightly smaller than the seasonal average. However, the snow coverage and ice melting of the two epochs led to the underestimation of our elevation change and velocity results, which need further investigation.

Keywords: glacier change detection; terminus retreat; unmanned aerial vehicle; photogrammetry

1. Introduction

Mountain glaciers are one of the most sensitive indicators of global climate change [1,2]. Recent studies have revealed that most mountain glaciers have experienced significant ablation and mass loss under global warming, which is particularly severe around the Southeastern Qinghai–Tibet Plateau (SETP) [3–8]. The rise in air temperatures and the persistent ablation of glaciers have changed their extents, surface velocity, and mass balances, leading to a series of glacier-related disasters, such as ice avalanches, glacial lake expansion, flooding, and glacial debris flows [9–13]. However, rapid changes in glaciers not only affect the surrounding natural and human systems but also have an impact on agricultural and tourism activities. Therefore, glacier monitoring plays an important role

in understanding glacier changes and preventing the hazards associated with glacier ablation. It is also essential for assessing water resources and sustainable development in glacierized regions [14,15].

There are several methods available for glacier monitoring, such as in situ measurements, satellite remote sensing, and unmanned aerial vehicle (UAV) surveys. These methods can be used to extract glacier change data, such as mass balance, ice volume, area, surface velocity, and glacier retreat, of which the in situ measurements use ablation stakes and GNSS receivers but cover only a limited spatial extent. Moreover, in a harsh environment, it is usually difficult to collect continuous data [15–18]. Furthermore, optical, radar, and microwave data are also often used for ice velocity [19,20]. Optical images have rough spatial resolution and are prone to cloud cover and shadows [16,21,22]. The latter two methods collect data regardless of weather conditions but are limited in data availability, spatial resolution, and shadow effects [20,23,24]. Therefore, satellite remote sensing methods may be less suitable for small mountain glaciers, especially those with complex terrains. UAVs can overcome many shortcomings associated with these methods. High-resolution images collected by UAVs can be employed to obtain digital elevation models (DEMs) and digital orthophoto maps (DOMs) [25,26], which are often used in glaciological studies, such as for glaciers, surface debris, ice cliffs, and ice-surface lakes [27–31]. In High-Mountain Asia, UAVs have been used to understand the dynamic features of glacier surfaces using repeated UAV photogrammetry and are often utilized around the Himalayas and the Qinghai–Tibet Plateau (QTP) [32–35]. Though several studies on UAV monitoring glaciers have been conducted in the QTP [36–39], there have been few special studies on glacier change detection in the SETP.

The SETP is located on the Southeastern QTP, with an average elevation of more than 4000 m. A total of 11,875 glaciers larger than 1 ha have been identified on the SETP, one-fifth of all QTP glaciers [40,41]. They provide water resources for rivers, which supply important water for people in East and South Asia [42]. Glaciers in the SETP have undergone important mass loss in recent decades, with a rate about three times higher than that observed across the entire QTP [43–45]. For example, glacier mass balance ranged from −0.30 m w.e./a to −0.11 m w.e./a in the southeastern QTP from the mid-1970s to 2000 compared with the northwestern part, with a mass balance range of −0.11 m w.e./a to 0.02 m w.e./a [8]. Because of abundant precipitation and low temperatures, there are a lot of marine glaciers across the SETP [45]. The terminus of these glaciers usually descends to lower elevations, resulting in severe ablation and an increase in the number of glacial lakes on the SETP [46].

Baishui River Glacier No. 1 (BRG1) is a typical temperate glacier in the SETP and the largest reference glacier of Yulong Snow Mountain (YSM), the closest temperate glacier area in the Eurasian continent to the Equator [47]. The state of the glacier is usually considered a representative indicator of local climate change, and its beautiful geological landscapes are also a valuable tourist resource [48]. To monitor the changes in BRG1, research has been conducted over the past decades. Previous studies have shown that BRG1 experienced notable ablation between 1982 and 2016, leading to the retreat of its terminus elevation from 4100 to 4300 m [49]. Moreover, observations indicate that the length of the glacier decreased from 2.65 to 1.90 km from 1957 to 2017, while the area decreased from 207 to 132 ha [48]. In addition, it was found that the area decreased by 36%, and the corresponding cumulative mass losses exceeded 32.38 ± 3.62 m w.e. over the 1951–2020 period [50]. Additionally, seasonal surface velocity and mass balance over a part of the debris regions in BRG1, covering only 6.1% of the total area, were revealed by repeat UAV flights in May and September 2018 [24,51].

These studies have focused on in situ or UAV data acquired during the ablation season, so there is still a lack of yearly results. So, two UAV surveys with larger coverage were performed on 20 October 2018 and 22 July 2021, as shown in Figure 1c. The data from these two surveys were used to derive DOMs and DEMs. In this paper, the yearly

elevation variation and velocity were further derived, and their spatial distribution was analyzed. The results were compared with the seasonal results of [24].
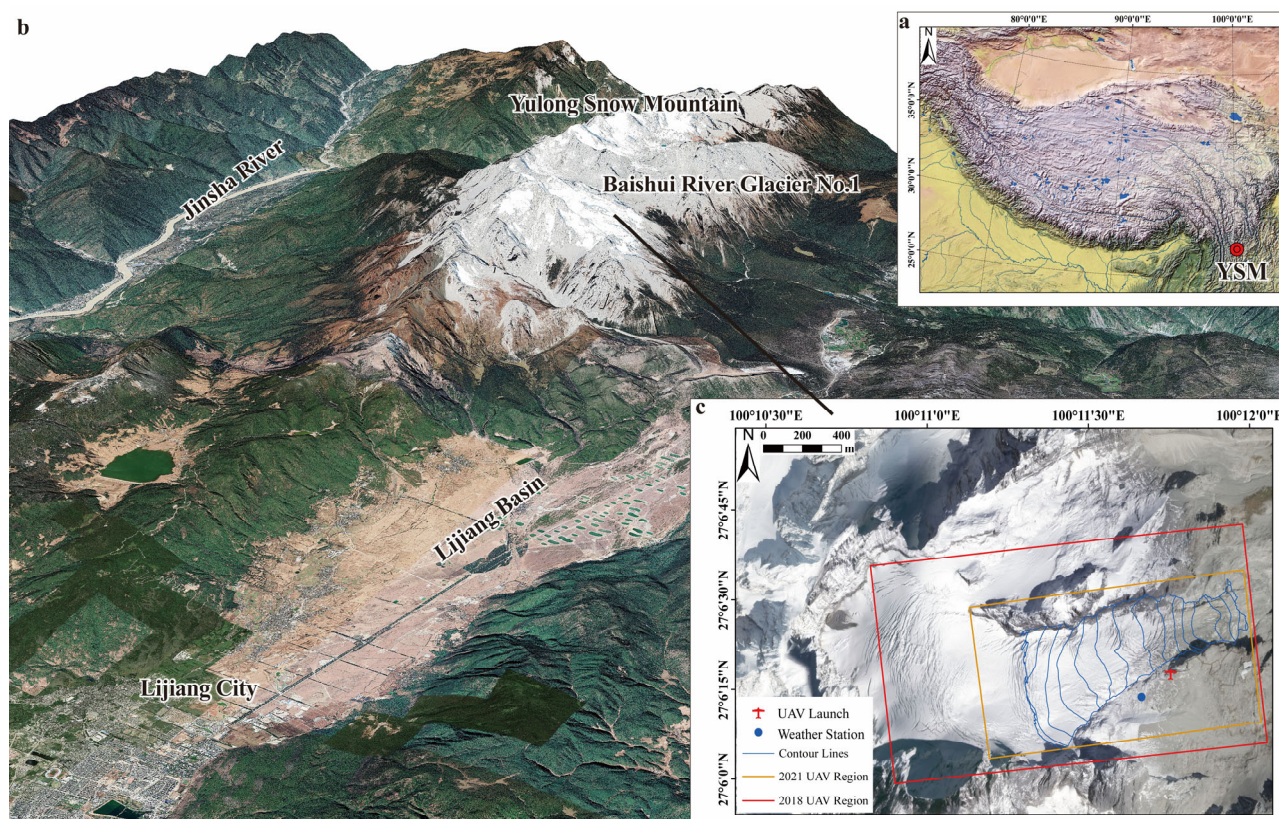
Figure 1. (**a**) Yulong Snow Mountain is located in the Southeastern Qinghai–Tibetan Plateau and the southern end of the Hengduan Mountains. (**b**) The location of Baishui River Glacier No. 1 on Yulong Snow Mountain. (**c**) Baishui River Glacier No. 1, the areas of different unmanned aerial vehicle surveys (the 2018 survey is shown as a red rectangle, and the 2021 survey is shown as a yellow rectangle), and the position where unmanned aerial vehicles were launched.

2. Study Site

Situated on the SETP, Yulong Snow Mountain (YSM) is a typically temperate glacier area [52]. YSM (26°59′–27°17′ N, 100°04′–100°15′ E) is located in the Southeastern QTP, about 25 km north of Lijiang City, as shown in Figure 1a [50,53]. It is influenced by the Indian and southeastern monsoons during the summer and autumn seasons, while dominated by the southern branch of the westerly wind belt during the winter and spring. Meanwhile, the average temperature in summer and autumn, 5.08 °C, is notably higher than −3.67 °C in winter and spring. Precipitation is predominantly concentrated during the warm seasons from June to September, accounting for 80–90% of the annual precipitation [24,53]. It spans an area of 13 km from east to west and 35 km from north to south, with its highest peak at 5596 m [48]. In 2017, there were 13 glaciers on the eastern slope of YSM, covering a total area of 448 ha [50]. These glaciers vary in elevation, ranging from 4395 to 5361 m [48], of which BRG1 is the largest on the east slope with a length of about 1.9 km, covering an area of around 132 ha, as shown in Figure 1b [48,54]. It represents a typical temperate glacier with a relatively broad firn basin, active crevasses in the glacier tongue area, and a steep terminal slope [55].

3. Data Collection and Data Analysis

3.1. UAV Surveying

The first survey was conducted on 20 October 2018 with the DJI Inspire 2, which has a maximum flight time of about 25 min at altitudes from 2500 to 5000 m, equipped with the DJI ZENMUSE X7 lens. The drone can hover and take a photo in the air with a labeled horizontal accuracy of ±0.3 m and vertical accuracy of ±0.1 m [56]. On 22 July 2021, the DJI M300 RTK (Real-Time Kinematic) was used, which has better wind resistance. It was equipped with the laser sensor ZENMUSE L1, which integrates a high-precision inertial navigation and mapping camera. Compared with the former drone, the DJI M300 RTK has a maximum altitude of 7000 m and a maximum flight time of 55 min in an operating temperature range of −20 °C to 50 °C. The horizontal and vertical accuracies are about 1 cm + 1 ppm and 1.5 cm + 1 ppm, respectively [57].

Given the terrain variation at BRG1, the flight altitude of the two drones was adjusted to maintain a consistent height above the surface. It was about 300 m above the take-off point, as shown in Figure 1c. We captured 200 and 97 images in 2018 and 2021, respectively. The Ground Sample Distance of each survey was 13.32 cm/pixel and 8.21 cm/ pixel, respectively. The coverage in 2018 was about 111 ha or 84% of the total BRG1 area when the glacier surface was partly covered with snow. The area in 2021 was about 63 ha, representing 47% of the total BRG1 area.

3.2. Processing of UAV Data

In this study, images were processed to DEMs and DOMs with Agisoft PhotoScan software v1.2.5. The process is as follows:

(1) Inputting each photograph and using the orientation and position of each photograph to generate a sparse point cloud model;

(2) Calculating the depth information of each camera with the MVS algorithm, merging them into a dense point cloud model, and then generating DEM and DOM images.

We finally obtained two DOMs and two DEMs with better spatial resolution in 2021 because of the different equipment and lenses. The resolutions of the DOMs and DEMs in 2021 were 0.1 and 0.22 m compared with 0.2 and 0.5 m in 2018. Hence, we resampled the DOMs and DEMs in 2021 to the same resolution in 2018. The nearest-neighbor method was used, and we obtained two DEMs and two DOMs with the same resolution.

3.3. Elevation Change Rate Calculation and Terminus Retreat Estimation of BRG1

As shown in Figure 2a, BRG1 has experienced glacier retreat, characterized by the disappearing ice region. Within this region, the ice has disappeared within different time spans, and hence, it is difficult to derive the elevation change rate. As shown in Figure 2b, we further divided the area into two parts: Area1, the disappeared region from 2018 to 2021, and Area2, determined by the terminus in 2021. For Area2, the elevation change rate was derived from the two DEMs.
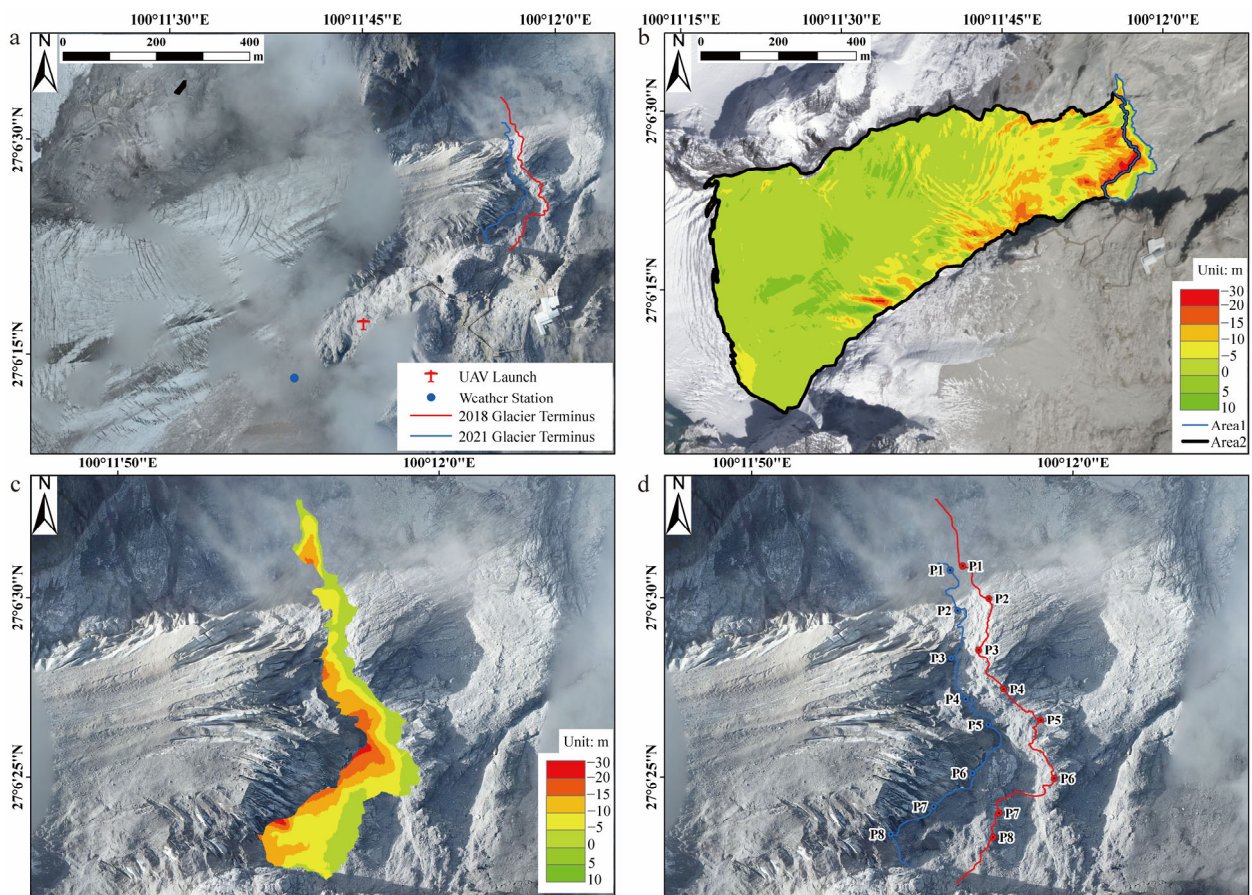
Figure 2. (**a**) Terminus of Baishui River Glacier No. 1 in 2018 and 2021; (**b**) elevation changes in Baishui River Glacier No. 1 from 20 October 2018 to 22 July 2021—Area1 is enclosed by the blue line, and Area2 is enclosed by the black line; (**c**) elevation change in Area1; (**d**) 8 selected feature points from glacier terminus.

For Area1, elevation change and advance/retreat (AR) were applied to show its changes. Three methods, the mainstream line method, the perimeter method, and the feature point method, are often used to derive AR position changes in glacier terminuses [58]. The mainstream line method determines the AR distance by considering changes in the glacier's mainstream line, while the perimeter method calculates it based on the area and the perimeter of this rectangle. The AR distance is calculated based on selected feature points at the glacier terminus and averaged by the feature point method. In this study, the AR results from the three algorithms were compared and evaluated.

3.4. Surface Velocity Calculation

Two methods are often used to calculate surface velocity from two images: one is the matching algorithm via automatic determination and the other is manual tracking by identifying homologous points between two images. For the former, ImGRAFT is one of the most useful tools for glacier surface velocity calculation in various regions, such as Greenland, the Alps, the Himalayas, and Tibetan Plateau regions [38,59–61]. Moreover, ImGRAFT enables rapid velocity determination based on the feature-matching algorithm [62].

In this study, two methods were used to calculate surface velocity. ImGRAFT was first employed to calculate surface velocity based on the DOMs, and the matching parameters are shown in Table A1. However, ImGRAFT failed to produce a reliable result, as shown in Figure A1, which may be due to the long time interval and different snow cover

conditions. Hence, we chose manual tracking to derive ice velocity by selecting homologous points from two DOMs.

4. Results

4.1. Elevation Change and Terminus Retreat in BGR1

Based on the two DEMs, we calculated the elevation difference between the two epochs, as shown in Figure 2b. There exists an overall lowering of the surface elevation due to glacial melting, with a minimum of −28.74 m and a maximum of 9.45 m. Moreover, strong elevation decreases were observed along the crevasse edges. The average surface elevation change from 2018 to 2021 was estimated to be −4.26 m. Based on the time difference of the two epochs, we further calculated an average change rate of −1.55 m/a.

To show the spatial variation in the elevation changes, we divided BGR1 into two sub-regions with a threshold of 4520 m a.s.l, with the lower less than 4520 m and the upper otherwise [63]. At the upper zone of BRG1, crevasses are present and more often observed in the south than the north, as shown in Figure 2b. Table 1 summarizes the statistics of the two sub-regions and the study area. The regional maximum and minimum elevation changes in the upper zone were about 9.22 and −24.11 m. The lower experienced a significant decrease, with a maximum and minimum of 9.95 and −28.74 m, respectively. This shows that the maximum of the upper is similar to that of the lower but with a minimum of only −24.11 m. This leads to the lower experiencing more ice loss than that of the upper. Moreover, the mean and the mean rate of the lower are about −8.81 m and −3.20 m/a, which is about 2.93 times that of the upper. Based on the DEMs and the terminus lines, we further estimated the elevation change in Area1, as shown in Figure 2c. Moreover, the elevation change from 2018 to 2021 was about −9.09 m.

Table 1. Statistics of elevation change in Baishui River Glacier No. 1.

| Region	Maximum (m)	Minimum (m)	Mean (m)	Mean Rate (m/a)
Study Area	9.95	−28.74	−4.26	−1.55
Lower	9.95	−28.74	−8.81	−3.20
Upper	9.22	−24.11	−3.01	−1.10

We further calculated the AR distances with three methods for Area1. For the feature point method, we selected eight feature points with equal distances along the terminus line, as shown in Figure 2d. The AR distances were estimated and are summarized in Table 2. It shows that the results from the mainstream line (−45.21 m) and the feature point method (−44.70 m) were consistent, with the negative representing the retreat of the glacier. The perimeter produced only ~60% of them, which may be related to the high-degree curvature of the terminus in BGR1. Compared with the mainstream line method, the feature point method has more details in spatial variation. Spatial variation was also observed at the eight points, with a minimum retreat of −11.19 m and a maximum of −87.95 m. Moreover, the minimum was observed in the north, while the maximum was observed in the south, showing that the AR distance varied with latitude.

Table 2. Advance/retreat distances from different methods.

| Method	Feature Point									Mainstream Line	Perimeter
AR (m)	Point 1	Point 2	Point 3	Point 4	Point 5	Point 6	Point 7	Point 8	Mean	−45.21	−26.93
	−11.19	−28.54	−24.37	−33.67	−45.10	−70.33	−56.43	−87.95	−44.70		
Rate (m/a)	−16.25									−16.44	−9.79

4.2. Glacier Surface Velocity Estimate

The DOMs are shown in Figure 3. The area in 2018 was about 1.11 km², which is much larger than the 0.63 km² of 2021. As mentioned in Section 3.4, the surface velocity could not be derived with ImGRAFT. For the low-velocity glacier, the ice velocity was derived using the high-correlation relationship between the surface velocity and elevation gradient [64–66]. In this study, we tried to evaluate the relationship between surface velocity and elevation gradient in the high-velocity glacier BRG1.
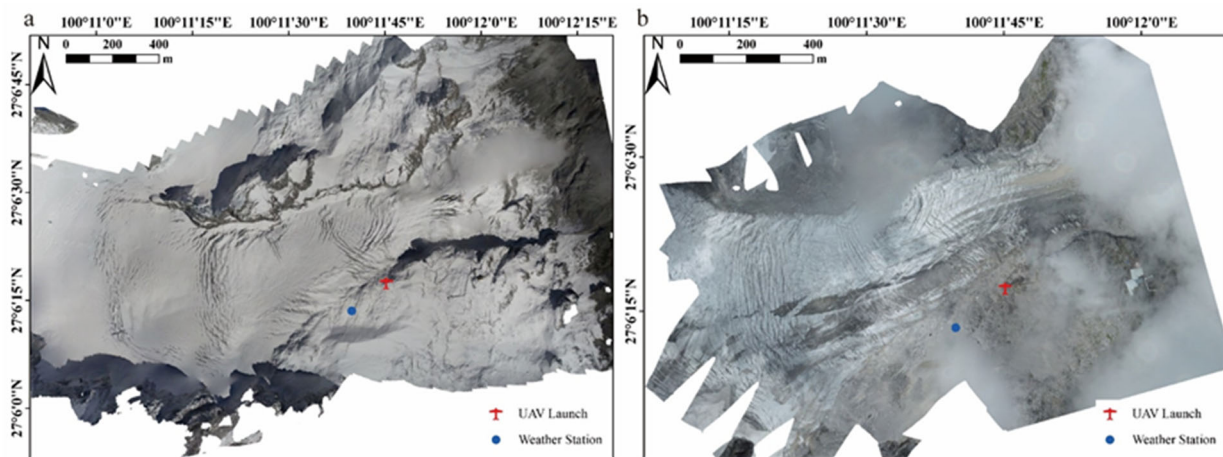
Figure 3. Digital orthophoto maps acquired in (**a**) 2018 and (**b**) 2021.

The surface velocity and elevation gradient of the lower region of BRG1 were provided in [24]. As shown in Figure A2, 151 homologous points were selected, and the surface velocity and gradient were extracted. Then, a simple linear relationship was fitted to the data. The high correlation between the gradient and surface velocity in BRG1 was found to be 0.90, indicating that this relationship can be used to derive the surface velocity of BRG1.

We can further demonstrate this relationship with our data in a larger area. Twelve evenly distributed homologous points were first selected, and the surface velocity and corresponding gradients were extracted. A similar correlation coefficient, 0.91, was derived, indicating, again, that this relationship can be used to derive the surface velocity of BRG1. The linear equation between them was fitted and is shown in Figure 4b, where the gradient increases by 0.1, and the velocity increases by ~1.13 m/a.
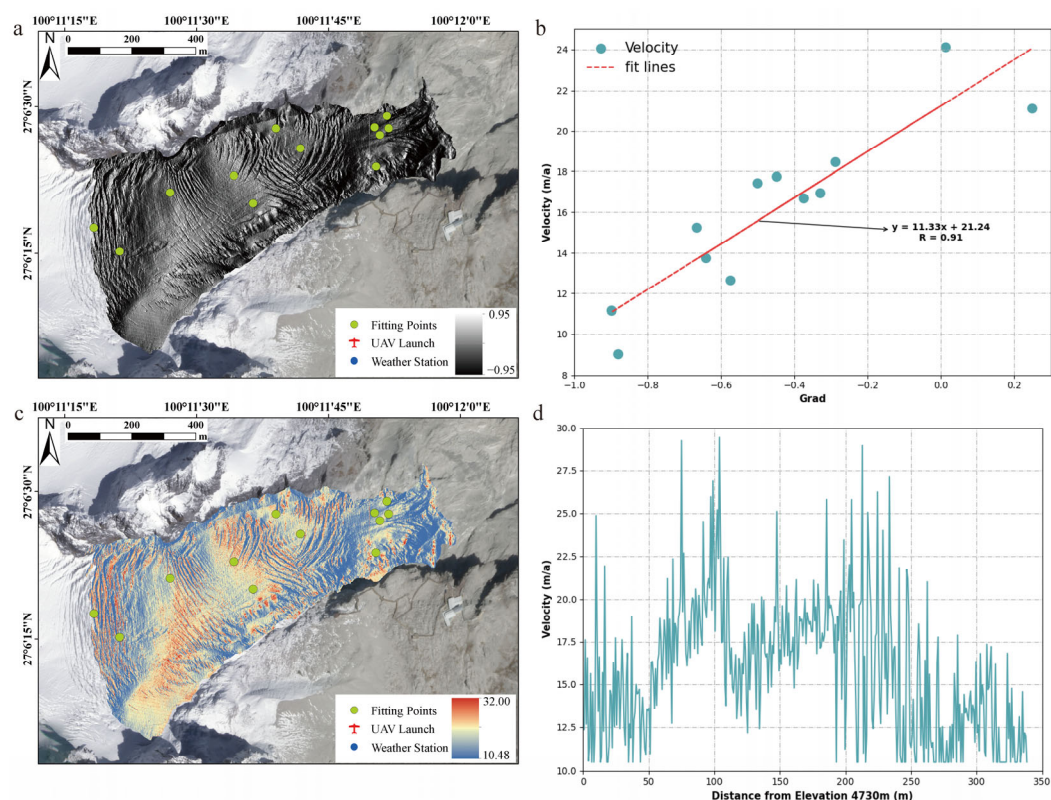
Figure 4. (**a**) Gradient of study area; (**b**) relationship between surface velocity and gradient; (**c**) derived surface velocity; (**d**) the surface velocity along the mainstream line.

The surface velocity was derived from the linear relationship and is shown in Figure 4c. It is shown that the surface velocities ranged from 10.48 to 32.00 m/a, with an average value of 15.76 m/a. Moreover, the surface velocity along the mainstream line is shown in Figure 4d, with a minimum of 10.48 m/a, a maximum of 29.43 m/a, and an average of 15.88 m/a. We found that the ice velocity along the mainstream fluctuates, with high surface velocities around the ice crevasses, which is similar to the results along the mainstream found by Yan between 2016 and 2017 [67]. Furthermore, the crevasses move faster close to the mainstream line than they do close to the glacier boundary.

5. Discussions and Conclusions

5.1. Error Analysis of Elevation Change and Surface Velocity

As shown in Figure 3a, the surface was covered by snow on 20 October 2018. Moreover, the surface ice decreased from 22 July to 20 October 2018. Hence, the decreased ice and snow depth of the surface may induce an elevation change error. In this step, we used the precipitation data to show the impact of snow coverage on the potential error of the elevation change results. Meteorological data from 22 July to 20 October 2018 were used, as shown in Figure 5a.
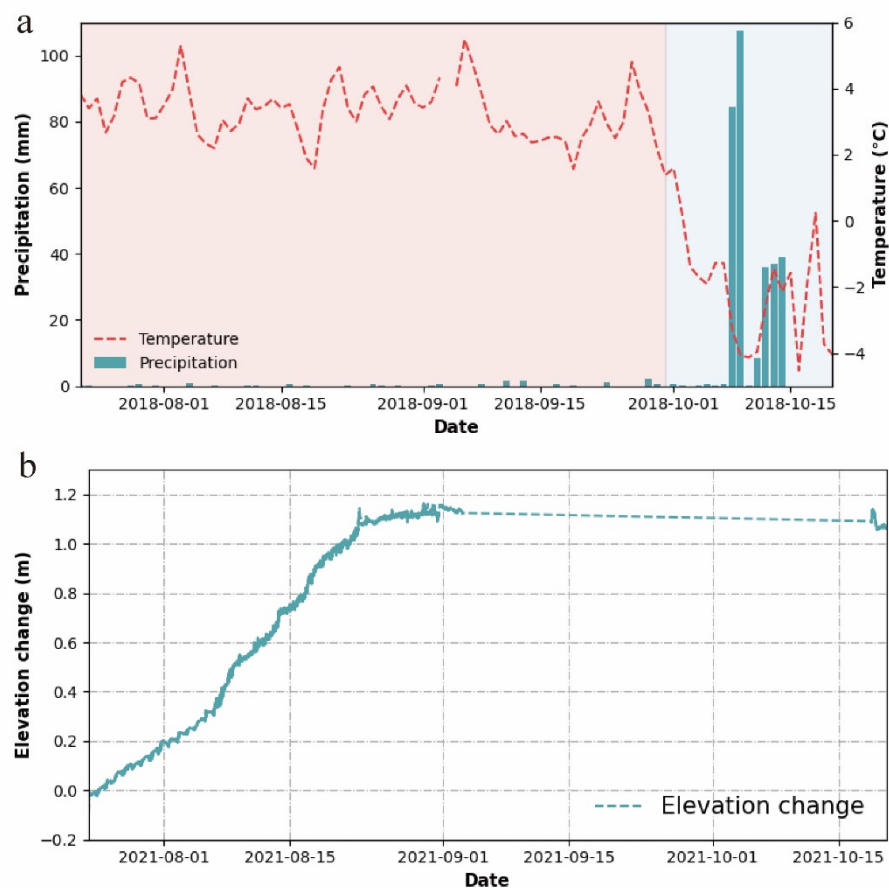
Figure 5. (**a**) The precipitation and temperature data collected between 22 July and 20 October 2018 from the meteorological station. (**b**) Surface elevation data between 22 July and 20 October 2021 from a real-time platform.

The temperature before 1 October 2018 fluctuated between 2 and 5 °C, with an average of about 3 °C. Then, the temperature decreased, falling to a negative value after 3 October. Snow was recorded starting on 3 October, with a daily average of 17.48 mm and a peak of 104.47 mm on 5 October. Using these data, the potential maximum snow depth of this period was estimated as 0.31 m based on the snow accumulation.

The temperature was higher than 0 °C before 1 October 2018, and the ice melted then. However, there were no surface elevation data derived from our UAV survey, so it is hard to show the elevation change between 22 July and 1 October 2018. Fortunately, we established a real-time monitoring platform on BRG1 in 2021, where surface elevation decrease data were recorded between July and October 2021 [47]. Here, we assumed that the elevation change in BRG1 between 22 July and 1 October 2018 was the same as in 2021. Subsequently, we substituted the 2021 BRG1 elevation change for the 2018 elevation change to calculate the error in elevation change due to the missing elevation information for 2018. Figure 5b shows a time series of elevation changes between 22 July and 20 October 2021, as derived by our real-time monitoring platform, indicating an obvious decrease. Although there were no data recorded between 3 September and 20 October 2021, the surface elevation was almost the same on 2 September and 18 October 2021. We simply calculated the decreased elevation as 1.08 m from the recording between 22 July and 2 September 2021. Given the snow accumulation results from the meteorological station and surface elevation data from the real-time monitor platform, we think the yearly surface elevation from the two UAVs was underestimated by about 0.77 m, and this was used as the potential error.

We further evaluated the potential error of the surface velocity. As the surface velocity was derived from the relationship between velocity and the elevation gradient, the rate of their linear equation is key. The study by Che computed the 2018 summer velocity of BRG1 but did not examine its correlation with gradients. Here, based on the data from [24], we established a linear relationship between velocity and gradients for the summer of 2018. The rate was derived as 29.85, as shown in Figure A2. We selected 40 homologous points in Figure A2 and extracted the relationship between velocity and gradients for these points in 2018–2021. The rate was derived as 20.42, as shown in Figure A3a. This means that our rate is about 0.68 of that of [24], leading to an underestimation of the surface velocity. Table A2 shows the results and the mean from 10 points calculated based on DOMs from September 2018 [24] to July 2021 and this study. For example, the mean velocities of Che and this study are 24.52 m/a and 18.02 m/a, respectively. The difference may be due to a higher speed in the summer. Our results indicate that the yearly velocity of BRG1 is less than the summer velocity. However, the results from the real-time monitoring platform on BRG1 show that there is no obvious seasonal change in the speed. This requires further investigation.

5.2. Relationship between Elevation Change and the Elevation

Temperature is the main factor affecting glacier ablation in YSM. As it normally decreases by 0.6 °C for every 100 m of elevation [68], we further investigated the relationship between elevation change and elevation. The pace of the elevation was set as 20 m, and the elevation change of each section was extracted. We finally obtained 16 sets, and all elevations experienced an elevation decrease, as shown in Figure 6a. Moreover, there was a strong relationship between the elevation change and elevation, with a correlation coefficient of 0.93. A positive rate of 0.036 was derived and is shown in Figure 6a, showing the larger elevation change in the lower elevation. For example, the elevation of 4700 m decreases by about −1.0 m from 2018 to 2021, while 4400 m changes by −11 m, indicating less ice mass loss in the higher region. A similar elevation change pattern has also been observed on glaciers in the Himalayas and the Alps, with annual mean mass balance change rates with elevations of 0.69 m w.e. and 0.78 m w.e. per 100 m, respectively [69,70]. The annual rate of elevation change in BRG1 is about 1.3 m per 100 m of elevation. This indicates that elevation change in BRG1 is more sensitive and drastic with respect to elevation.
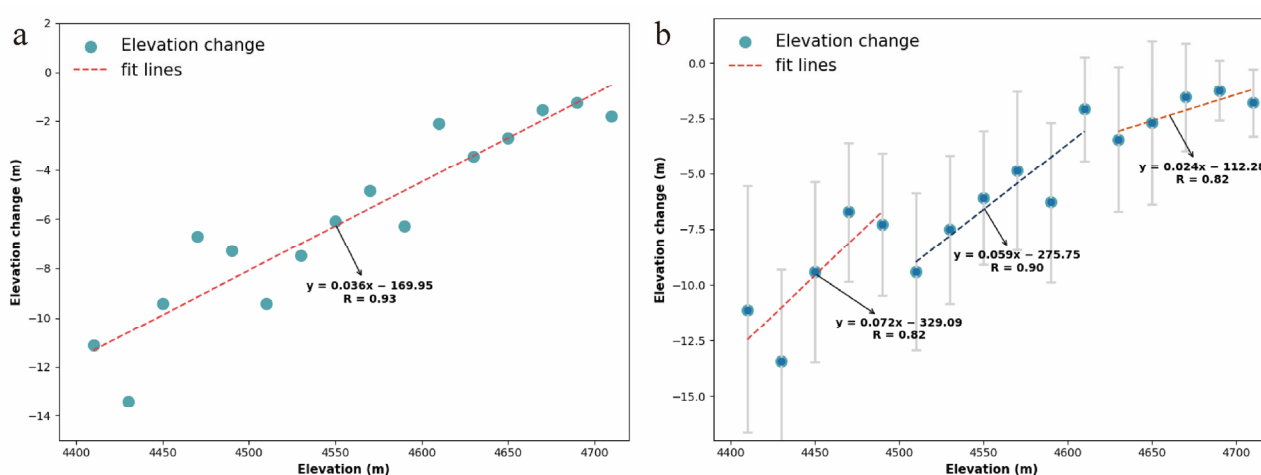
Figure 6. (**a**) Relationship between elevation and elevation change; (**b**) elevation change distribution along the elevation in different regions.

We further analyzed the elevation changes in three regions separated by elevation every 100 m. The fitting rate between elevation change and elevation was derived for the three regions, as shown in Figure 6b. Moreover, high correlation coefficients, 0.82, 0.90,

and 0.82, were again derived for these regions. The rates were 0.072, 0.059, and 0.024, respectively, showing that they decrease with increasing elevation. The depiction of BRG1's mass loss rate with elevation also illustrates the weakening of snow and ice melt with elevation because of lower temperatures at higher elevations.

5.3. Conclusions

In this study, we conducted two repeated UAV surveys of BRG1's ablation area, covering about 84% and 47% of BRG1. Using these UAV images, 0.20 m DOMs and 0.50 m DEMs were derived and used to derive the ice velocity and elevation change of two epochs.

The elevation of BRG1 between 2018 and 2021 experienced severe ablation, and its surface elevation is still dropping. Moreover, the lower part of BRG1 lost more ice than other areas. However, the snow coverage and ice melting of the two epochs led to an error, and it is shown that our results underestimated the elevation change. We calculated the AR distance of the BRG1 terminus using three different methods and found that the AR distance shows spatial variation with latitude. In addition, the results obtained using the perimeter method were small compared with the other two methods, which may be related to the high-degree curvature of the terminus in BGR1.

Moreover, the automatic matching algorithm failed to produce ice surface velocity. It was found that there was a high correlation between surface velocity and the elevation gradient in this high-speed glacier. The surface velocity was calculated using the manual feature tracking method. We established the relationship between the gradient and surface velocity and derived the velocity. We found the ice velocity along the mainstream fluctuates, with higher surface velocities around the ice crevasses. Compared with the automatic matching algorithm, the ice velocity results may have been underestimated by the manual feature tracking method.

Author Contributions: Methodology, L.L.; validation, L.L. and C.W.; formal analysis, L.L.; resources, L.L., Y.Y., S.W., Yanjun Che, and J.W.; investigation, L.L., Y.Y., S.A. and Yuqiao Chen; data curation, L.L. and Q.W.; writing—original draft preparation, L.L.; writing—review and editing, L.L.; supervision, Y.Y.; funding acquisition, Y.Y. All authors have read and agreed to the published version of the manuscript.

Data Availability Statement: Data are contained within the article.

Conflicts of Interest: The authors declare no conflicts of interest.
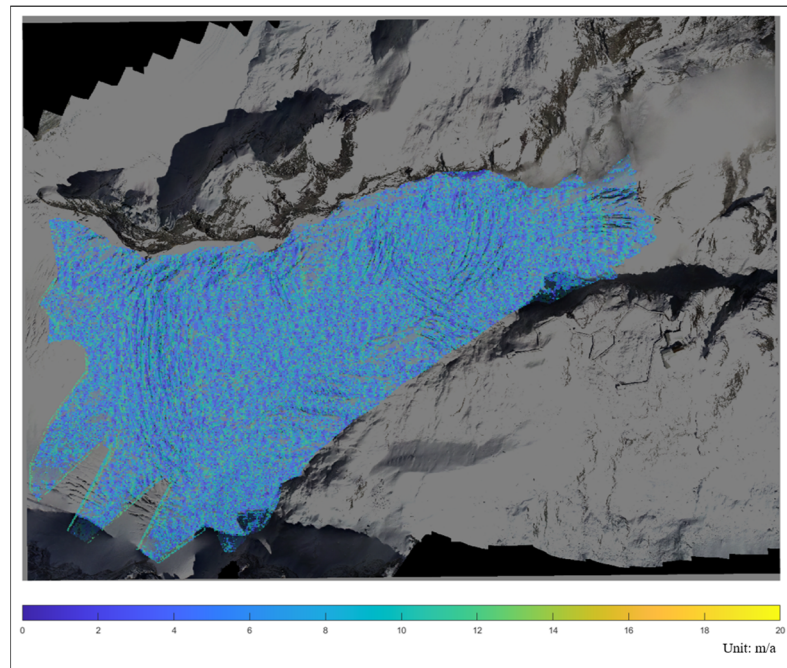
Appendix A

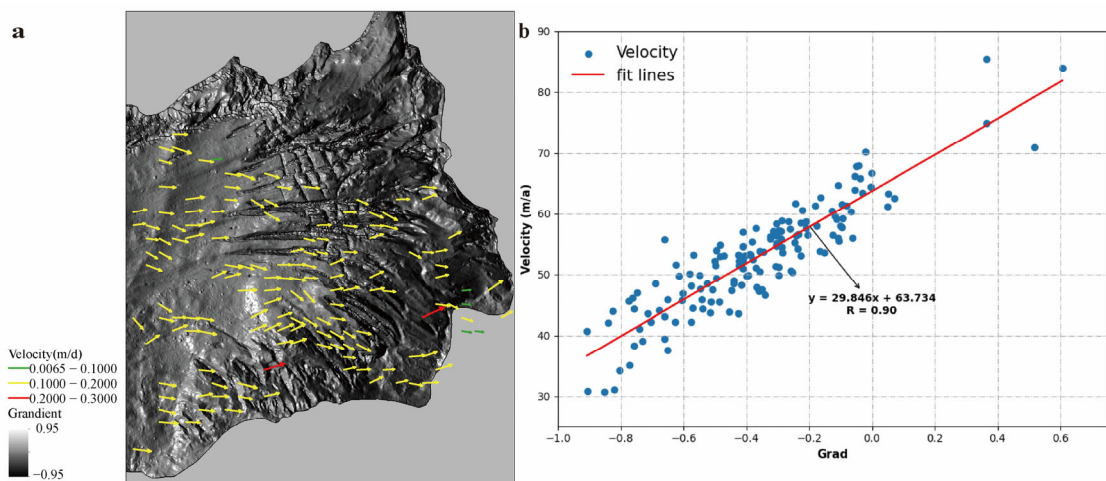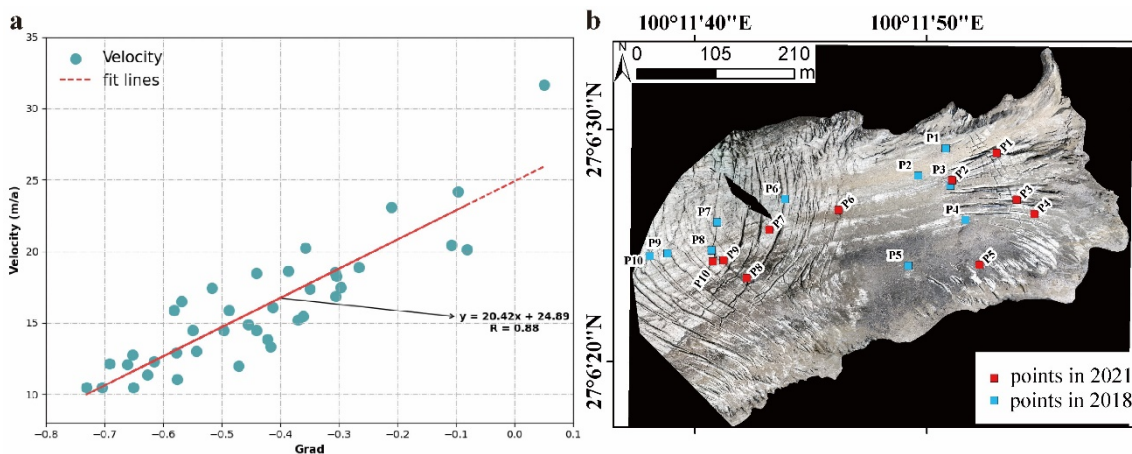**Figure A1.** Glacier surface velocity extracted by ImGRAFT.

Figure A2. (**a**) The 151 homologous points selected; (**b**) relationship between velocity and elevation gradient.

Figure A3. (**a**) Relationship between velocity and elevation gradient of 40 points selected from Figure A2; (**b**) the selected homologous points: red points represent 2021, and blue points represent 2018.

Table A1. Parameters used in ImGRAFT for this study.

Figures	A1
Data source	DJI UAV
Data resolution	0.2 m
Grid resolution	2 m
Template window size	30 pixels
Search window size	150 pixels

Table A2. Velocity difference between Che's results and ours.

Points	Point 1	Point 2	Point 3	Point 4	Point 5	Point 6	Point 7	Point 8	Point 9	Point 10	Mean
Velocity of Che (m/a)	22.07	15.25	28.71	30.01	30.76	23.69	22.75	20.21	24.49	27.30	24.52
Velocity of ours (m/a)	16.40	11.29	23.31	21.59	21.71	17.67	16.94	13.73	17.65	19.93	18.02
Difference (m/a)	5.67	3.96	5.39	8.42	9.05	6.02	5.80	6.48	6.84	7.37	6.50

References

1. Yanjun, C.; Mingjun, Z.; Zhongqin, L.; Shuang, J.; Wenbin, W.; Shengjie, W. Understanding the mass balance characteristics of Qingbingtan Glacier No. 72 during the period of 2008–2014. *J. Glaciol. Geocryol.* **2020**, *42*, 318–331.
2. Friedl, P.; Seehaus, T.; Braun, M. Global time series and temporal mosaics of glacier surface velocities derived from Sentinel-1 data. *Earth Syst. Sci. Data* **2021**, *13*, 4653–4675. https://doi.org/10.5194/essd-13-4653-2021.
3. Wang, Y.; Zhao, J.; Li, Z.; Zhang, M.; Wang, Y.; Liu, J.; Yang, J.; Yang, Z. Retrieving and Verifying Three-Dimensional Surface Motion Displacement of Mountain Glacier from Sentinel-1 Imagery Using Optimized Method. *Water* **2021**, *13*, 1793. https://doi.org/10.3390/w13131793.
4. Pang, H.; He, Y.; Zhang, N.; Li, Z.; Theakstone, W.H. Observed glaciohydrological changes in China's typical monsoonal temperate glacier region since 1980s. *J. Earth Sci.* **2010**, *21*, 179–188. https://doi.org/10.1007/s12583-010-0016-1.
5. Bhambri, R.; Hewitt, K.; Kawishwar, P.; Pratap, B. Surge-type and surge-modified glaciers in the Karakoram. *Sci. Rep.* **2017**, *7*, 15391.
6. Gardelle, J.; Berthier, E.; Arnaud, Y. Slight mass gain of Karakoram glaciers in the early twenty-first century. *Nat. Geosci.* **2012**, *5*, 322–325.
7. Sun, M.; Liu, S.; Yao, X.; Guo, W.; Xu, J. Glacier changes in the Qilian Mountains in the past half-century: Based on the revised First and Second Chinese Glacier Inventory. *J. Geogr. Sci.* **2018**, *28*, 206–220.
8. Zhou, Y.; Li, Z.; Li, J.; Zhao, R.; Ding, X. Glacier mass balance in the Qinghai–Tibet Plateau and its surroundings from the mid-1970s to 2000 based on Hexagon KH-9 and SRTM DEMs. *Remote Sens. Environ.* **2018**, *210*, 96–112. https://doi.org/10.1016/j.rse.2018.03.020.
9. Millan, R.; Mouginot, J.; Rabatel, A.; Jeong, S.; Cusicanqui, D.; Derkacheva, A.; Chekki, M. Mapping Surface Flow Velocity of Glaciers at Regional Scale Using a Multiple Sensors Approach. *Remote Sens.* **2019**, *11*, 2498. https://doi.org/10.3390/rs11212498.
10. Wang, W.; Yao, T.; Yang, X. Variations of glacial lakes and glaciers in the Boshula mountain range, southeast Tibet, from the 1970s to 2009. *Ann. Glaciol.* **2011**, *52*, 9–17.
11. Veh, G.; Korup, O.; Walz, A. Hazard from Himalayan glacier lake outburst floods. *Proc. Natl. Acad. Sci. USA* **2020**, *117*, 907–912.
12. Kääb, A.; Leinss, S.; Gilbert, A.; Bühler, Y.; Gascoin, S.; Evans, S.G.; Bartelt, P.; Berthier, E.; Brun, F.; Chao, W.-A. Massive collapse of two glaciers in western Tibet in 2016 after surge-like instability. *Nat. Geosci.* **2018**, *11*, 114–120.
13. Wei, R.; Zeng, Q.; Davies, T.; Yuan, G.; Wang, K.; Xue, X.; Yin, Q. Geohazard cascade and mechanism of large debris flows in Tianmo gully, SE Tibetan Plateau and implications to hazard monitoring. *Eng. Geol.* **2018**, *233*, 172–182.
14. Che, Y.; Zhang, M.; Li, Z.; Li, H.; Wang, S.; Sun, M.; Zha, S. Glacier mass-balance and length variation observed in China during the periods 1959–2015 and 1930–2014. *Quat. Int.* **2017**, *454*, 68–84.
15. Immerzeel, W.W.; Kraaijenbrink, P.D.A.; Shea, J.M.; Shrestha, A.B.; Pellicciotti, F.; Bierkens, M.F.P.; de Jong, S.M. High-resolution monitoring of Himalayan glacier dynamics using unmanned aerial vehicles. *Remote Sens. Environ.* **2014**, *150*, 93–103. https://doi.org/10.1016/j.rse.2014.04.025.
16. Nascetti, A.; Nocchi, F.; Camplani, A.; Di Rico, C.; Crespi, M. Exploiting Sentinel-1 Amplitude Data for Glacier Surface Velocity Field Measurements: Feasibility Demonstration on Baltoro Glacier. *ISPRS-Int. Arch. Photogramm. Remote Sens. Spat. Inf. Sci.* **2016**, *XLI-B7*, 783–788. https://doi.org/10.5194/isprsarchives-XLI-B7-783-2016.
17. Moragues, S.N.; Lenzano, M.G.; Lo Vecchio Repetto, A.; Falaschi, D.; Lenzano, L.E. Surface velocities of Upsala glacier, Southern Patagonian Andes, estimated using cross-correlation satellite imagery: 2013–2014 period. *Andean Geol.* **2018**, *45*, 87–103.

18. Wang, P.; Li, Z.; Xu, C.; Xing, W.; Zhou, P.; Zhang, H. Multi-decadal variations in glacier flow velocity and the influencing factors of Urumqi Glacier No. 1 in Tianshan Mountains, Northwest China. *J. Arid Land* **2017**, *9*, 900–910. https://doi.org/10.1007/s40333-017-0067-6.

19. Shi, Y.; Liu, G.; Wang, X.; Liu, Q.; Shum, C.K.; Bao, J.; Mao, W. Investigating the Intra-Annual Dynamics of Kunlun Glacier in the West Kunlun Mountains, China, From Ascending and Descending Sentinel-1 SAR Observations. *IEEE J. Sel. Top. Appl. Earth Obs. Remote Sens.* **2022**, *15*, 1272–1282. https://doi.org/10.1109/jstars.2022.3142990.

20. Whitehead, K.; Moorman, B.; Hugenholtz, C. Brief Communication: Low-cost, on-demand aerial photogrammetry for glaciological measurement. *Cryosphere* **2013**, *7*, 1879–1884.

21. Wang, P.; Li, H.; Li, Z.; Liu, Y.; Xu, C.; Mu, J.; Zhang, H. Seasonal Surface Change of Urumqi Glacier No. 1, Eastern Tien Shan, China, Revealed by Repeated High-Resolution UAV Photogrammetry. *Remote Sens.* **2021**, *13*, 3398.

22. Ke, L.; Song, C.; Yong, B.; Lei, Y.; Ding, X. Which heterogeneous glacier melting patterns can be robustly observed from space? A multi-scale assessment in southeastern Tibetan Plateau. *Remote Sens. Environ.* **2020**, *242*, 111777.

23. Wu, K.; Liu, S.; Jiang, Z.; Xu, J.; Wei, J. Glacier mass balance over the central Nyainqentanglha Range during recent decades derived from remote-sensing data. *J. Glaciol.* **2019**, *65*, 422–439.

24. Che, Y.; Wang, S.; Yi, S.; Wei, Y.; Cai, Y. Summer Mass Balance and Surface Velocity Derived by Unmanned Aerial Vehicle on Debris-Covered Region of Baishui River Glacier No. 1, Yulong Snow Mountain. *Remote Sens.* **2020**, *12*, 3280. https://doi.org/10.3390/rs12203280.

25. Xue, Y.; Jing, Z.; Kang, S.; He, X.; Li, C. Combining UAV and Landsat data to assess glacier changes on the central Tibetan Plateau. *J. Glaciol.* **2021**, *67*, 862–874.

26. Bash, E.A.; Moorman, B.J. Surface melt and the importance of water flow–an analysis based on high-resolution unmanned aerial vehicle (UAV) data for an Arctic glacier. *Cryosphere* **2020**, *14*, 549–563.

27. Wu, K.; Liu, S.; Zhu, Y.; Xie, F.; Gao, Y. High-resolution monitoring of glacier dynamics based on unmanned aerial vehicle survey in the Meili Snow Mountain. *Prog. Geogr.* **2021**, *40*, 1581–1589. https://doi.org/10.18306/dlkxjz.2021.09.012.

28. Pieczonka, T.; Bolch, T. Region-wide glacier mass budgets and area changes for the Central Tien Shan between~ 1975 and 1999 using Hexagon KH-9 imagery. *Glob. Planet. Chang.* **2015**, *128*, 1–13.

29. Poblete, T.; Ortega-Farías, S.; Ryu, D. Automatic coregistration algorithm to remove canopy shaded pixels in UAV-borne thermal images to improve the estimation of crop water stress index of a drip-irrigated Cabernet Sauvignon vineyard. *Sensors* **2018**, *18*, 397.

30. Tonkin, T.N.; Midgley, N.; Cook, S.J.; Graham, D. Ice-cored moraine degradation mapped and quantified using an unmanned aerial vehicle: A case study from a polythermal glacier in Svalbard. *Geomorphology* **2016**, *258*, 1–10.

31. Rossini, M.; Di Mauro, B.; Garzonio, R.; Baccolo, G.; Cavallini, G.; Mattavelli, M.; De Amicis, M.; Colombo, R. Rapid melting dynamics of an alpine glacier with repeated UAV photogrammetry. *Geomorphology* **2018**, *304*, 159–172. https://doi.org/10.1016/j.geomorph.2017.12.039.

32. Kraaijenbrink, P.; Meijer, S.W.; Shea, J.M.; Pellicciotti, F.; De Jong, S.M.; Immerzeel, W.W. Seasonal surface velocities of a Himalayan glacier derived by automated correlation of unmanned aerial vehicle imagery. *Ann. Glaciol.* **2016**, *57*, 103–113.

33. Brun, F.; Wagnon, P.; Berthier, E.; Shea, J.M.; Immerzeel, W.W.; Kraaijenbrink, P.D.; Vincent, C.; Reverchon, C.; Shrestha, D.; Arnaud, Y. Ice cliff contribution to the tongue-wide ablation of Changri Nup Glacier, Nepal, central Himalaya. *Cryosphere* **2018**, *12*, 3439–3457.

34. van Woerkom, T.; Steiner, J.F.; Kraaijenbrink, P.D.; Miles, E.S.; Immerzeel, W.W. Sediment supply from lateral moraines to a debris-covered glacier in the Himalaya. *Earth Surf. Dyn.* **2019**, *7*, 411–427.

35. Racoviteanu, A.E.; Glasser, N.F.; Robson, B.A.; Harrison, S.; Millan, R.; Kayastha, R.B.; Kayastha, R. Recent evolution of glaciers in the Manaslu region of Nepal from satellite imagery and UAV data (1970–2019). *Front. Earth Sci.* **2022**, *9*, 767317.

36. Xue, Y.; Jing, Z.; Kang, S. Application of unmanned aerial vehicle in glacier change monitoring: Taking the Xiao Dongkemadi Glacier in the Tanggula Mountains as an example. *Prog. Geogr.* **2021**, *40*, 1590–1599.

37. Chuanxi, Z.; Wei, Y.; Yongjie, W.; Baohong, D.; Xinchang, X. Changes in surface elevation and velocity of Parlung No. 4 glacier in southeastern Tibetan Plateau: Monitoring by UAV technology. *J. Beijing Norm. Univ.* **2020**, *56*, 557–565.

38. Liu, Y.; Qin, D.; Jin, Z.; Li, Y.; Xue, L.; Qin, X. Dynamic Monitoring of Laohugou Glacier No. 12 with a Drone, West Qilian Mountains, West China. *Remote Sens.* **2022**, *14*, 3315.

39. Yang, W.; Zhao, C.; Westoby, M.; Yao, T.; Wang, Y.; Pellicciotti, F.; Zhou, J.; He, Z.; Miles, E. Seasonal Dynamics of a Temperate Tibetan Glacier Revealed by High-Resolution UAV Photogrammetry and In Situ Measurements. *Remote Sens.* **2020**, *12*, 2389.

40. RGI 7.0 Consortium. *Randolph Glacier Inventory—A Dataset of Global Glacier Outlines, Version 7.0*; NSIDC: National Snow and Ice Data Center: Boulder, CO, USA, 2023. https://doi.org/10.5067/f6jmovy5navz.

41. Xiao, Y.; Ke, C.-Q.; Cai, Y.; Shen, X.; Wang, Z.; Nourani, V.; Lhakpa, D. Glacier Retreating Analysis on the Southeastern Tibetan Plateau via Multisource Remote Sensing Data. *IEEE J. Sel. Top. Appl. Earth Obs. Remote Sens.* **2023**, *16*, 2035–2049.

42. Immerzeel, W.W.; Van Beek, L.P.; Bierkens, M.F. Climate change will affect the Asian water towers. *Science* **2010**, *328*, 1382–1385.

43. Brun, F.; Berthier, E.; Wagnon, P.; Kääb, A.; Treichler, D. A spatially resolved estimate of High Mountain Asia glacier mass balances from 2000 to 2016. *Nat. Geosci.* **2017**, *10*, 668–673.

44. Hugonnet, R.; McNabb, R.; Berthier, E.; Menounos, B.; Nuth, C.; Girod, L.; Farinotti, D.; Huss, M.; Dussaillant, I.; Brun, F. Accelerated global glacier mass loss in the early twenty-first century. *Nature* **2021**, *592*, 726–731.

45. Zhao, F.; Long, D.; Li, X.; Huang, Q.; Han, P. Rapid glacier mass loss in the Southeastern Tibetan Plateau since the year 2000 from satellite observations. *Remote Sens. Environ.* **2022**, *270*, 112853.

46. Wang, X.; Guo, X.; Yang, C.; Liu, Q.; Wei, J.; Zhang, Y.; Liu, S.; Zhang, Y.; Jiang, Z.; Tang, Z. Glacial lake inventory of high-mountain Asia in 1990 and 2018 derived from Landsat images. *Earth Syst. Sci. Data* **2020**, *12*, 2169–2182.

47. Wang, C.; Yang, Y.; Wang, S.; Ai, S.; Che, Y.; Wang, J.; Li, L.; Li, F. Seasonal glacier change revealed from the real-time monitoring platform on Baishui River Glacier No. 1 in Yulong Snow Mountain, Southeastern Qinghai–Tibet plateau. *Ann. Glaciol.* **2023**, 1–11. https://doi.org/10.1017/aog.2023.48.

48. Wang, S.; Che, Y.; Pang, H.; Du, J.; Zhang, Z. Accelerated changes of glaciers in the Yulong Snow Mountain, Southeast Qinghai-Tibetan Plateau. *Reg. Environ. Chang.* **2020**, *20*, 38. https://doi.org/10.1007/s10113-020-01624-7.

49. Pang, H.; Yuanqing, H.; Zhang, N. Accelerating glacier retreat on Yulong Mountain, Tibetan Plateau, since the late 1990s. *J. Glaciol.* **2007**, *53*, 317–319.

50. Yan, X.; Ma, J.; Ma, X.; Wang, S.; Chen, P.; He, Y. Accelerated glacier mass loss with atmospheric changes on Mt. Yulong, Southeastern Tibetan Plateau. *J. Hydrol.* **2021**, *603*, 126931. https://doi.org/10.1016/j.jhydrol.2021.126931.

51. Che, Y.; Wang, S.; Liu, J. Application of unmanned aerial vehicle (UAV) in the glacier region with complex terrain: A case study in Baishui River Glacier No. 1 located in the Yulong Snow Mountains. *J. Glaciol. Geocryol.* **2019**, *41*, 1–9.

52. Yang, W.; Yao, T.; Xu, B.; Ma, L.; Wang, Z.; Wan, M. Characteristics of recent temperate glacier fluctuations in the Parlung Zangbo River basin, southeast Tibetan Plateau. *Chin. Sci. Bull.* **2010**, *55*, 2097–2102. https://doi.org/10.1007/s11434-010-3214-4.

53. Yan, X.; Ma, J.; Ma, X.; Chen, P.; Wang, S.; Wei, Y.; Zhu, G.; Zhang, W. Hydrothermal combination and geometry control the spatial and temporal rhythm of glacier flow. *Sci. Total Environ.* **2021**, *760*, 144315. https://doi.org/10.1016/j.scitotenv.2020.144315.

54. Du, J.; He, Y.; Li, S.; Wang, S.; Niu, H.; Xin, H.; Pu, T. Mass balance and near-surface ice temperature structure of Baishui Glacier No.1 in Mt. Yulong. *J. Geogr. Sci.* **2013**, *23*, 668–678. https://doi.org/10.1007/s11442-013-1036-4.

55. Liu, L.; Jing, Z. A Study of Velocity of Baishui No. 1 Glacier, Mt. Yulong. *Adv. Earth Sci.* **2012**, *27*, 987.

56. DJI-Innovation. Inspire-2 User Manuals. Available online: https://www.dji.com/inspire-2 (accessed on 31 July 2019).

57. DJI-Innovation. Matrice-300 RTK User Manuals. Available online: https://www.dji.com/matrice-300 (accessed on 29 July 2022).

58. Li, P.; Yan, M.; Xu, Y.; Liu, L.; Zhang, Y. Calculation Methods of Glacier Terminus Variation Based on GIS: A Case Study on Austre Lovénbreen in Arctic. *J. Glaciol. Geocryol.* **2012**, *34*, 367–374.

59. Miles, E.; Quincey, D.J.; Miles, K.; Hubbard, B.P.; Rowan, A.V. Quantifying seasonal velocity at Khumbu Glacier, Nepal. In Proceedings of the AGU Fall Meeting Abstracts, New Orleans, LA, USA, 11–15 December 2017; pp. C51D–05.

60. Ahsan, M.H. *Dynamics and Evolution of Iconic Glaciers in Southern Alps of New Zealand*; Politecnico di Torino: Turin, Italy, 2022.

61. Messerli, A.; Karlsson, N.B.; Grinsted, A. No slowing down of Jakobshavn Isbræ in 2014: Results from feature-tracking five Greenland outlet glaciers using Landsat-8 data and the ImGRAFT toolbox. In Proceedings of the EGU General Assembly Conference Abstracts, Vienna, Austria, 12–17 April 2015; p. 9857.

62. Messerli, A.; Grinsted, A. Image georectification and feature tracking toolbox: ImGRAFT. *Geosci. Instrum. Methods Data Syst.* **2015**, *4*, 23–34. https://doi.org/10.5194/gi-4-23-2015.

63. Jiankuo, D.; Shuang, L.; Shuxin, W. Analysis of the surface velocity characteristics of Baishui Glacier No.1, Yulong Mountain. *J. Yunnan Univ. Nat. Sci. Ed.* **2019**, *41*, 317–322. https://doi.org/10.7540/j.ynu.20180149.

64. Cuffey, K.M.; Paterson, W.S.B. *The Physics of Glaciers*; Academic Press: Cambridge, MA, USA, 2010.

65. Yang, Y.; Sun, B.; Wang, Z.; Ding, M.; Hwang, C.; Ai, S.; Wang, L.; Du, Y.; E, D. GPS-derived velocity and strain fields around Dome Argus, Antarctica. *J. Glaciol.* **2017**, *60*, 735–742. https://doi.org/10.3189/2014JoG14J078.

66. Liu, T.; Niu, M.; Yang, Y. Ice velocity variations of the polar record glacier (East Antarctica) using a rotation-invariant feature-tracking approach. *Remote Sens.* **2017**, *10*, 42.

67. Xingguo, Y. *The Mass Balance and Surface Velocity of Baishui River Glacier No.1 in Yulong Snow Mountain*; Northwest Normal University: Lanzhou, China, 2018.

68. Barry, R.G. *Mountain Weather and Climate*; Routledge: Oxfordshire, UK, 2013.

69. Wagnon, P.; Linda, A.; Arnaud, Y.; Kumar, R.; Sharma, P.; Vincent, C.; Pottakkal, J.G.; Berthier, E.; Ramanathan, A.; Hasnain, S.I. Four years of mass balance on Chhota Shigri Glacier, Himachal Pradesh, India, a new benchmark glacier in the western Himalaya. *J. Glaciol.* **2007**, *53*, 603–611.

70. Rabatel, A.; Dedieu, J.-P.; Vincent, C. Using remote-sensing data to determine equilibrium-line altitude and mass-balance time series: Validation on three French glaciers, 1994–2002. *J. Glaciol.* **2005**, *51*, 539–546.